www.tubiad.org
ISSN:2148-3736
El-Cezerî Fen ve Mühendislik Dergisi
Cilt: 1, No: 3, 2014

El-Cezerî Journal of Science and Engineering
Vol: 1, No: 3, 2014

ECJSE

Makale / Research Paper

Depth Normalization Algorithm for Continuous Wave Reflectance Diffuse Optical Tomography System

Hüseyin Özgür Kazancı, Murat Canpolat*

Biomedical Optic Research Unit, Department of Biophysics, Medical School, Akdeniz University, Antalya 07058, Turkey
canpolat@akdeniz.edu.tr

Depth Normalization Algorithm for Continuous Wave Reflectance Diffuse Optical Tomography System

Abstract: Continuous wave reflectance diffuse optical tomography (CWRDOT) systems incapable for accurate depth localization, since physical nature of light. We have used a new approach to calculate the unknown optical properties of breast like tissue by getting weight data from Monte Carlo (MC) simulation codes. In this work, we have developed a depth normalization algorithm (DNA), which normalizes weight matrix elements for each source and detector couplings for separate depth layers. Banana functions for source-detector pairs have been created by multiplying individual fluence rates of each source and detectors. Then, the weight coefficients of the voxels in volume have been used in inverse problem solution with the Tikhonov regularization method to obtain absorption and scattering coefficients for each voxel of tissue phantoms. Tikhonov regularization method has been used as an inverse problem solution to reconstruct the tissue phantom concentrations. It has been shown that a contrast-to-noise ratio (CNR) is 0.85 to 2 depends on the depth of the inclusion and the average position error over all the depths between 0 to 4 cm are 12.5 %.

Keywords: Diffuse optical tomography system; inverse problem solution; Monte Carlo (MC) simulation; depth normalization algorithm (DNA).

1. Introduction

Continuous wave reflectance diffuse optical tomography (CWRDOT) systems have been under investigation to be used in clinics for brain or breast imaging. CWRDOT has been most interested imaging modality in the last decade as a way of imaging tissue up to depths of 3-4 cm for different source and detector placement geometry and techniques [1,2]. Error and contrast analysis methods have been also investigated for CWRDOT systems [3]. Light propagate by diffusing in tissue due to scattering of photons; there is not a unique defined trajectory to be used in image reconstruction. Distribution of the light within the tissue depends on scattering and absorption properties. It has been shown that in reflection geometry measurements, distribution of the photon trajectories between source and detector positions look like a banana shape [4-7]. Reconstruction of tissue

Bu makaleye atıf yapmak için
Kazancı, HO, Canpolat M, *"Depth normalization algorithm for continuous wave reflectance diffuse optical tomography system"* El-Cezerî Fen ve Mühendislik Dergisi 2014, Cilt(1); sayfa.

How to cite this article
Kazancı, HO, Canpolat M, "*Depth normalization algorithm for continuous wave reflectance diffuse optical tomography system*" El-Cezerî Journal of Science and Engineering, 2014, Vol.(1); pages.

image requires solution of inverse problem. Different methods have been used to reconstruct the tissue chromophores via the absorption distribution within a region of interest (ROI). The most common method is the Radiative Transfer Equation (RTE) or linear Rytov approximation to the electromagnetic wave propagation in random media according to Maxwell equations [8], in which diffuse optical images are taken using Tikhonov regularization method. Different geometries of sources and detectors for better resolution had been studied for experimental and theoretical. The fluence rate of light decreases rapidly by depth, therefore perturbation of an inclusion from deeper tissue is less than superficial. Due to high weight of the voxels close to the surface, location of an inclusion shifts toward to surface. Recently, a depth compensation algorithm (DCA) was developed to overcome this negative effect [9] and has been used in simulation studies and in vivo experiments to accurately localize an absorber within tissue [10-12]. In the algorithm, the depth compensation parameter requires to estimate actual depth of an inclusion. Therefore, an adjuvant system like magnetic resonance imaging or ultrasound is required to estimate depth compensation parameter.

2. Method

In the presented study, Monte Carlo (MC) simulation to define fluence rates for each voxel within a volume of 3.9x3.9x3.9 cm^3 defined by $\mu_a = 0.04$ cm^{-1}, $\mu_s' = 10$ cm^{-1} for tissue background. Photon fluxes were translated for each source and the detector positions of the probe geometry to be able to build weight matrix from MC simulations to real geometry problem. MC simulations have been run according to specific radial distance and depth. There are totally 30 radial and 15 depth steps. In the reconstruction process while simulation data has been transferred into reconstruction medium voxel sizes and distributions have not been the same as in MC simulation. In the reconstruction process 26x26x16 xyz steps have been used. There was a geometry mismatch between simulation and real problem. Closest distances have been used as data have been translated to real geometry to figure out photon fluence rates. In the MC simulation, fluence rates had been acquired from source to voxel and voxel to detector positions. Then for each source-detector pairs weight functions have been obtained by multiplying the fluence rates of the sources and the detectors positions. Fluence rate multiplication product values have been accepted for each voxel as their weights. Novel method have been used which normalizes weight matrix in the same depth layer for specific source-detector coupling by dividing the all voxel values of the same layer to their maximum value. Using CWRDOT system with the same fiber probes geometry was originally designed as a chess board which has 49 sources and 49 detectors, data were acquired from a tissue phantom with the same optical properties of the MC simulation. The tissue phantom CWRDOT measurements were performed with and without inclusions. Perturbation vector was calculated by the ratio of particle measurement data divided over non-particle measurement data and direct subtraction of the measurements. These are the first type of perturbation vectors which have been used for inverse problem solution. The weight matrix obtained from the MC simulation were used in the Tikhonov regularization inverse problem solution. Experimental measurements of matrix of source-to-detector light transport values yield data in counts. Perturbation data is the perturbed signal P. Both perturbed signal method P1 and P2 has been used.
M(is,id,it) [counts], Measurement data

is = the is_{th} source
id = the id_{th} detector
it = the it_{th} integration time
mask = (Mnp – Mwp) > 0 [Boolean]
perturbed signal P1 = (Mnp/Mwp)*mask [counts]
perturbed signal P2 = (Mnp – Mwp)*mask [counts]
Mnp = no particles measurement data in tissue
Mwp = with particles measurement data in tissue

To prepare fluence rate multiplication product $\Phi_{in}\Phi_{out}$ from MC simulation codes: First of all 2 dimension (2D) MC simulations have been run for different radial distances and different depths to yield optical fluence rates, $\Phi(r,z)$ [W/cm^2 per W delivered] or (1/cm^2), using radially symmetric grid for breast like tissue example. In MC simulation codes absorption coefficient $\mu_a = 0.04$ cm^{-1}, and scattering coefficient $\mu_s' = 10$ cm^{-1} have been used for tissue background. For experimental intralipid setup tissue properties were $\mu_a = 0$ cm^{-1}, $\mu_s' = 10$ cm^{-1}. In the MC simulation codes tissue properties were close to real values. After running MC simulation, weight matrix calculation program have been used which converges $\Phi(r,z)$ into three dimension (3D) map of Φ_{in} from each source to all positions within tissue grid for each voxel position. Program also converges $\Phi(r,z)$ into 3D map of Φ_{out} from all voxel positions within tissue grid to each detector position. Then the product $\Phi_{in}\Phi_{out}$ yields photon visiting functions for collected photons from each source-detector pair. The "visiting function" is the joint probability of transport form the source position to a tissue voxel coordinate and transport from that voxel coordinate to the detector position. In here, first goal has been accomplished and finally the functions which have been looked for have been represented and described as 3D "banana" shape functions. The result is:
$\Phi_{in}\Phi_{out}$(is,id,ix,iy,iz) [cm^{-4}]

is, id = the is$_{th}$ source, the id$_{th}$ detector
ix = number of voxels in x direction
iy = number of voxels in y direction
iz = number of voxels in z direction

Figure 1 shows a typical banana shape photon visiting function $T_{in}T_{out}$:

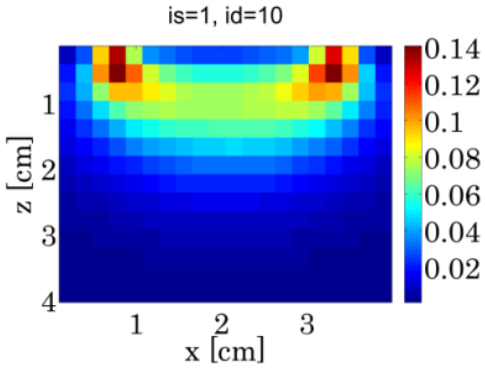


Fig. 1. Typical banana shape photon visiting function.

Using $\Phi_{in}\Phi_{out}$ to fill transport matrix ΦΦ could be shown that the $\Phi_{in}\Phi_{out}$(is,id,iy,ix,iz) is reshaped into matrix ΦΦ:

ΦΦ(Nsd,Nxyz) : Transport matrix
Nsd = Ns*Nd : The total number of source-detector pairs
Nx : The total number of voxel points in x direction
Ny : The total number of voxel points in y direction
Nz : The total number of voxel points in z direction
Nxyz = Nx*Ny*Nz: Number of voxels in tissue phantom

This ΦΦ matrix connects the measurement data M [counts] to the each voxel. In other words, expressed as a matrix equation:

P(jsd) = ΦΦ(jsd,ixyz)*$\Delta\mu_a$(ixyz)*V
P = ΦΦ*($\Delta\mu_a$V)

jsd : j_{th} source-detector coupling
ixyz : i_{th} voxel
ΦΦ : transport weight matrix
$\Delta\mu_a$: unknown voxel absorption concentrations
V : volume of each voxel

Tissue phantom experiments have been used in 3 steps. In step 1 $\Delta\mu_a V$ have been solved with using Tikhonov regularization for experimental data. To solve for the perturbing absorption in each voxel, $\Delta\mu_a(ixyz)*V$ [cm^2], the above matrix ΦΦ is multiplied by its transpose matrix to yield a square matrix, then multiplied by its inverted matrix so as to solve for the unknown vector of perturbing absorption within each voxel, $\Delta\mu_a V$.

$P = \Phi\Phi*(\Delta\mu_a V)$
$\Phi\Phi^T P = \Phi\Phi^T\Phi\Phi*(\Delta\mu_a V)$
$(\Phi\Phi^T\Phi\Phi)^{-1}* \Phi\Phi^T P = (\Phi\Phi^T\Phi\Phi)^{-1}*\Phi\Phi^T\Phi\Phi*(\Delta\mu_a V) = \Delta\mu_a V$

The above equation suffers from values too close to the zero. Tikhonov regularization adds a diagonal vector of positive values, which stabilizes the solution in Equation 1:

$$(\Phi\Phi^T\Phi\Phi + I\lambda)^{-1}\Phi\Phi^T P = \Delta\mu_a V \quad (1)$$

I = identity matrix
λ = regularization parameter, eg. ~ 6e+3

In step 2 we have performed additional method that aid for solution of experimental data. The above solution for $\Delta\mu_a V$ tends to be overly sensitive to superficially located absorbers, and insensitive to deeper absorbers. To compensate for this bias, the following protocol has been applied. First, xyz coordinate limits of banana shape have been defined. In these limits the size of ΦΦ has been reshaped into ΦΦ'(jsd,Nxy,iz), where jsd is the total number of source and detector couplings, Nxy is the total number of xy plane voxels in the same depth layer, iz is the total number of depth layers, so that for each source and detector pairs, all of the voxels in a given depth layer at iz are grouped, and normalized by the maximum value of the each group. Then the ΦΦ is reshaped back into a new ΦΦ matrix, ΦΦ"(jsd,ixyz) for use in the matrix equation. This protocol is summarized by for loop representation as in Matlab program:

```
for iz=1:Nz
        U=reshape(ΦΦ(jsd,:,:,iz),Nx*Ny,1)
        ΦΦ'(jsd,:,:,iz)=ΦΦ(jsd,:,:,iz)/max(U)
end
ΦΦ"(jsd,ixyz)=reshape(ΦΦ'(jsd,:,:),Nsd,Nx*Ny*Nz)
```

This ΦΦ" then has been substituted for ΦΦ before using the matrix equation 1.
In step 3 further averaging of the experimental data using common neighbors has been applied for experimental data as a second type of perturbation method. The experimental data, the perturbed signal P [counts], was somewhat noisy. Yet many of the source-detector pairs shared the same distance, d, between the source and the detector. Hence, in the absence of perturbations, the counts M(jsd) sharing a common d distance should have the same value. There were 22 such groupings of source and detector pairs with common values of d. The data of each of these groupings were averaged, and this mean value subtracted from the same distance data. Only P(jsd) that were truly perturbed persisted in showing a significant perturbed signal. By this method second type of perturbation have been applied inside the first one. The following representation is showing the method in Equation 2:

$$P''(jsd)_{common.d} = P(jsd) - mean(all\ P(jsd)_{common.d}) \quad (2)$$

This P" is then substituted for P before using in the matrix equation 1. Experiments were done with and without two indocyanine green (ICG) inclusions inside the intralipid tank and the P perturbation vector was used to solve inverse problem. The Figure 2 and Figure 3 shows the 3D reconstruction of two inclusion mini bubbles and their xz and xy intersections, respectively:

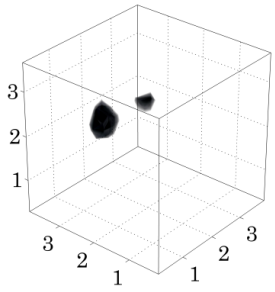


Fig. 2. 3D reconstruction image of two inclusions.

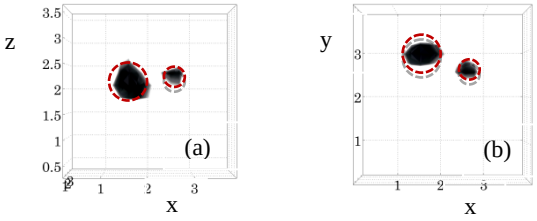


Fig. 3. Reconstruction of two inclusion mini bubbles (a) 2D xz view , (b) 2D xy view

In experiment, two mini (ICG) bubbles have been put inside the intralipid tank, 2cm depth and 1 cm away from each other with 1cm diameter. $\mu_a = 0.16\ cm^{-1}$, $\mu_s' = 10 cm^{-1}$. Images have been accurately reconstructed as shown in Figure 3(a) and 3(b). Beside the experiment, test procedure has also been applied for new model. For test purposes artificial data set have been used. Inclusions have been put into different depth positions. Then forward model has been created by matrix multiplication. Data have been calculated. Then Tikhonov regularization method for inverse problem solution has been applied. Figure 4 shows different inclusion localizations and their inverse problem solution replacements. Left is basic, right is DNA with Tikhonov reconstructed images. While basic Tikhonov method was getting deeper inclusion close to superficial, DNA method is solving real problem and getting correct position of inclusion.

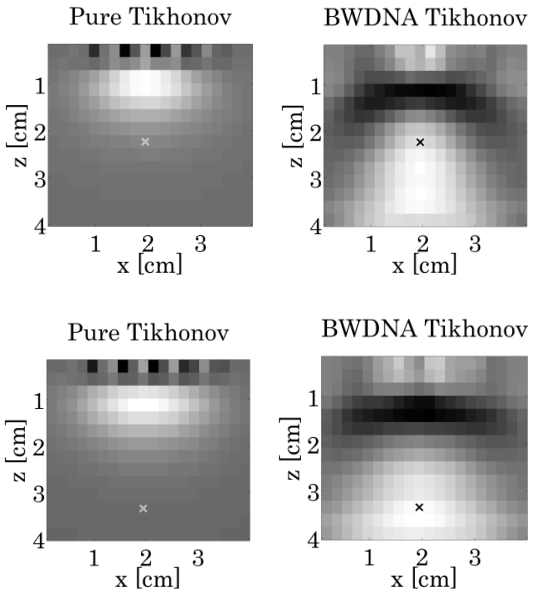


Fig. 4. 2D Reconstruction images of test inclusions for different x and z positions for pure Tikhonov (1a-2a) and for DNA (Depth Normalization Algorithm) Tikhonov (1b-2b) solution.

DNA has been applied first time for one of the CWRDOT system. This method is new and getting benefit from novel normalization algorithm. For each source and detector pairs, photons are traveling in tissue as banana shape. In literature, similar methods have also been shown for a long time ago. The inverse problem is solved in these literatures [7-8]. For each source and detector pairs, weight matrix for different depth layers have been normalized. By using this way negative importance effect of upper layer weights has been got rid off and equalized the importance of each layer. Before the normalization steps, there were photon fluence hotspots near to surface. But after normalization each layer weight importance has been equalized. Before applying DNA algorithm, hot spots can be seen close to source and detector surface of tissue geometry. If the retrieved data is used directly into the inverse problem regularization method, reconstructed images shift through to surface of the tissue. To counterbalance weight differences, new DNA method has been applied. Weights have been normalized and have been equalized. Contrast-to-noise ratio (CNR) and position error (PE) have been calculated as a function of different depths. The CNR was calculated using equation 3 as shown in below:

$$CNR = \frac{\mu_{ROI} - \mu_{bgn}}{\sqrt{w_{ROI}\sigma_{ROI}^2 + w_{bgn}\sigma_{bgn}^2}} \qquad (3)$$

$$w_{bgn} = {}^{A_{bgn}}\!/_{A_{tot}} \quad w_{ROI} = {}^{A_{ROI}}\!/_{A_{tot}}$$

where μ_{ROI} and μ_{bgn} represent the mean of the reconstructed absorption coefficient in the region of interest (ROI) and background, respectively. The σ_{ROI} and σ_{bgn} terms are the standard deviation of the reconstructed absorption coefficients in the ROI and background, respectively. The weights w_{bgn} and w_{ROI} represent the ratio of the areas of the background and ROI to the total area, respectively. As could be seen in Figure 5(a), the CNR is over average at deeper positions when the inclusion is far from the surface. The position error has been calculated according to following formula.

$$PE = \sqrt{(x_{real} - x_{recon})^2 + (z_{real} - z_{recon})^2} \qquad (4)$$

where (x_{real}, z_{real}) and (x_{recon}, z_{recon}) are the true xz coordinates and the reconstructed xz coordinates of the image of the inclusion. The PE has been calculated for different depths. The variation in the PE for the inclusion at different depths is shown in Figure 5(b).

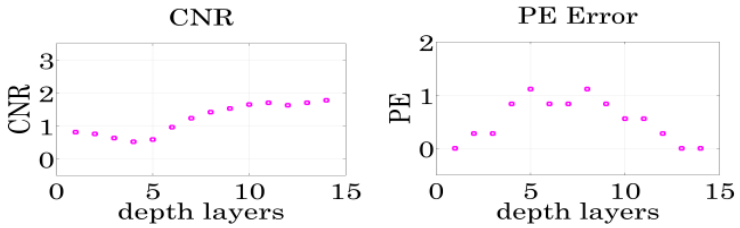


Fig. 5. (a) CNR vs. depth layers (b) PE vs. depth layers.

Novel method has been invented to construct the weight matrix of inverse problem solution space. This new method has helped to reconstruct the image in tissue with high CNR. By DNA method it is possible to get inclusion images correctly from deeper positions. Adjuvant imaging methods have not been used to support diffuse optical tomography imaging.

This work has been supported by the TUBITAK BIDEB 2214/A Grant.

References

[1] D. A. Boas, T. Gaudette, and S. R. Arridge, "Simultaneous imaging and optode calibration with diffuse optical tomography," Opt. Express **8**, 263-270 (2001).

[2] T. Yamamoto, A. Maki, T. Kadoya, Y. Tanikawa, Y. Yamad, E. Okada, and H. Koizumi, "Arranging optical fibres for the spatial resolution improvement of topographical images," Phys. Med. Biol. **47**, 3429-3440 (2002).

[3] X. Song, B. W. Pogue, S. Jiang, M. M. Doyley, H. Dehgani, T. D. Tosteson, and K. D. Paulsen, "Automated region detection based on the contrast to noise ratio in near infrared tomography," App. Opt. 43, 1053- 1062 (2004).

[4] W. Cui, C. Kumar, B. Chance, "Experimental study of migration depth for the photons measured at sample surface," Proc. SPIE 1431, 180-191 (1991).

[5] S. Feng, F. Zeng, B. Chance, Monte Carlo simulations of photon migration path distributions in multiple scattering media, Proc. SPIE 1888, 78-89 (1993).

[6] S. Feng, F. Zeng, and B. Chance, "Photon migration in the presence of a single defect a perturbation analysis," Appl. Opt. 34, 3826-3837 (1995).

[7] A.Yodh and B. Chance, "Spectroscopy and imaging with diffusion light", phys. Today, 48, 34-45 (1995).

[8] X.D. Zhu, S.Wei, S. C. Feng, B. Chance. "Analysis of a diffuse-photon-density wave in multiple-scattering media in the presence of a small spherical object", J.Opt.Soc.Am.A, 13, 494-499 (1996).

[9] H. J. Niu, F. Tian, Z.J. Lin, and H. Liu, "Development of a compensation algorithm for accurate depth localization in diffuse optical tomography," Opt. Lett. 35, 429-431 (2010).

[10] F. H. Tian, H. Niu, S. Khadka, Z. J. Lin, and H. Liu, "Algorithmic depth compensation improves quantification and noise suppresion in functional diffuse optical tomography," Biomed. Opt. Express 1, 441-452 (2010).

[11] H. J. Niu, Z. J. Lin, F. Tian, S. Dhamne, and H. Liu, "Comprehensive investigation of three-dimensional diffuse optical tomography with depth compensation algorithm," Biomed. Opt. 15, 046005 (2010).

[12] F. Liu, M. Li, B. Zhang, J. Luo, J. Bai, "Weighted depth compensation algorithm for Fluorescence molecular tomography Reconstruction," Appl. Opt. 36, 518883 (2012).